frontiers | Frontiers in Earth Science

TYPE Original Research
PUBLISHED 07 October 2025
DOI 10.3389/feart.2025.1654910

OPEN ACCESS

EDITED BY
George Kontakiotis,
National and Kapodistrian University of Athens, Greece

REVIEWED BY
Fayaz Ullah Shinwari,
Researches Organization for Develpment (ROD), Afghanistan
Imad Mahmood Ghafor,
University of Sulaymaniyah, Iraq
Salman Khattak,
The University of Haripur, Pakistan

*CORRESPONDENCE
Fudong Wang,
wolfdongswust@163.com

RECEIVED 27 June 2025
ACCEPTED 08 September 2025
PUBLISHED 07 October 2025

CITATION
He W, Wang F, Pérez-Mejías C, Capezzuoli E, Chen S, Wang Y, Zhu Y, Zhao X, Dong F, Zhang Q and Liu X (2025) Depositional constraints of sand-like calcium carbonate particles in the high-calcium cold springs of Huanglong, China: insights from mineralogy, geochemistry, and hydrodynamics .
Front. Earth Sci. 13:1654910.
doi: 10.3389/feart.2025.1654910

Depositional constraints of sand-like calcium carbonate particles in the high-calcium cold springs of Huanglong, China: insights from mineralogy, geochemistry, and hydrodynamics

Wuyang He[1], Fudong Wang[1]*, Carlos Pérez-Mejías[2], Enrico Capezzuoli[3], Shi Chen[1], Yanwen Wang[4], Yuyin Zhu[1], Xueqin Zhao[1], Faqin Dong[1], Qingming Zhang[5] and Xinze Liu[6]

[1]School of Environment and Resources, Southwest University of Science and Technology, Mianyang, China, [2]Institute of Global Environmental Change, Xi'an Jiao tong University, Xi'an, China, [3]Department of Earth Sciences, University of Florence, Florence, Italy, [4]State Key Laboratory of Earthquake Dynamics, Institute of Geology, China Earthquake Administration, Beijing, China, [5]Huanglong National Scenic Spot Administration, Songpan, Sichuan, China, [6]Sichuan Geological Environment Survey and Research Center, Chengdu, Sichuan, China

Calcium carbonate particles are common in many sedimentary environments, with the formational processes unresolved. Due to the variety of sedimentary environments, these particles exhibit significant variations in their petrographic, mineralogical, and geochemical features, as well as their genetic mechanisms. In the Huanglong travertine system, Sichuan, China, unique calcium carbonate particles, resembling sand grains, have been identified and are referred to as sand-like particles (0.5–3.0 mm). This study systematically investigates the mineralogical, petrographic, and geochemical characteristics of these particles. The particles form in a high-Ca^{2+} cold spring environment (Ca^{2+} >3.00 mM, T < 13 °C) through an exceptional aggregation-cementation-accretion-compaction process involving both detrital fragments and newformed calcite crystals. The particle growth is primarily controlled by hydrodynamic fluctuations and microbial mediation, with extracellular polymeric substances (EPS) templating calcite nucleation while kinetic disequilibrium drives rapid crystallization. These composite particles preserve distinct microtextural signatures of multiple diagenetic phases, offering new insights into non-classical carbonate formation. This study highlights the complexity and diversity of localized travertine deposition, bridging the gap between macroscopic sedimentary frameworks and localized depositional processes. The Huanglong system represents a unique natural laboratory for studying carbonate sedimentation under hydrochemical gradients. This research provides fundamental insights into the complex interplay between inorganic processes (hydrochemical precipitation driven by high Ca^{2+} and CO_2 degassing) and organic mediation (microbial activity and extracellular polymeric substances) in these unique high-calcium

aquatic systems. This not only elucidates the diversity of carbonate deposition mechanisms in Huanglong's environment, but also holds significant implications for understanding the establishment of similar coupled physicochemical-biological systems in other high-altitude, calcium-rich spring environments worldwide.

KEYWORDS

travertine system, high-calcium cold spring, sand-like particles, hydrodynamic force, Huanglong ravine

1 Introduction

Travertine and tufa, as described by Ford and Pedley (1996) and Pentecost (2005) secondary carbonate rocks formed by the deposition of karst waters in various environments such as springs, rivers, and lakes on the surface or in caves. These terrestrial carbonate rocks (Capezzuoli et al., 2014) are common in the Quaternary record (Pedley, 1990). The chemical deposition of continental travertine can be described by a gas -water-solid equilibrium reaction as follows: Ca^{2+} (aq) + 2 HCO_3^- (aq) ⇌ $CaCO_3$ (s) + H_2O (1) + CO_2 (g). Travertine landscapes have not only become prized tourism resources due to their aesthetic appeal, but more importantly, they have emerged as significant scientific archives with unique value for paleoclimate reconstruction and geological event documentation (Matsuoka et al., 2001; Garnett et al., 2004; Liu, 2014; Rodríguez-Berriguete et al., 2018; Tchouatcha et al., 2016; Gao et al., 2013; Temiz et al., 2021). As a result, the study of sedimentary environments and the evolution of travertine systems has become a major research focus (Amato et al., 2012; Croci et al., 2016; Henchiri et al., 2017; Kano et al., 2019; Qiu et al., 2022).

The Huanglong Scenic Area in Sichuan, China, represents an actively forming continental carbonate system, often described as a "natural travertine museum" due to its extensive and diverse travertine formations (Dong et al., 2023). The area features various carbonate landscapes, including travertine waterfalls, colorful pools with basins and side stone dams, beach flows, and caves (Lu and Li, 1992; Lu et al., 2000). During our investigation of the Huanglong travertine system, we observed notable accumulations of spherical or near-spherical calcium carbonate particles along the edges of rimstone dams adjacent to the pools, particularly in zones with low water flow and gentle slopes. Since these particles exhibit morphological and size characteristics similar to sand grains, they are herein referred to as "sand-like particles". Spherical or near-spherical calcium carbonate particles, such as pisoids, ooids, oncoids, pearls, spherulites, and vadoids, are found in various continental sedimentary environments, each with distinct characteristics and formation mechanisms (Folk and Chafetz, 1983; Verrecchia et al., 1995; Porta, 2015; Melim et al., 2009; Melim and Spilde, 2018; Mors et al., 2022). Their characteristics are strongly influenced by genetic conditions, with morphology, size and internal structure reflecting sedimentary environments.

Preliminary observations in Huanglong indicate that sand-like particles may compromise rimstone dam structural integrity and inhibit the natural evolution of travertine pools. These detrital particles (Guo, 2005; Zhang et al., 2012a), being highly susceptible to fluvial transport, predominantly accumulate along pool rear margins and dam peripheries. Such accumulations not only diminish the aesthetic value of travertine landscapes but also physically alter local hydrodynamic patterns through sediment loading, potentially redirecting flow paths and exacerbating asymmetric erosion. And may biochemically influence cementation processes via particle-associated microbial communities, thereby weakening structural cohesion. While these hypothesized mechanisms require validation through targeted monitoring, they underscore the critical need to elucidate particle formation mechanisms and their geomorphological roles in carbonate systems.

Historically, investigations of travertine systems have relied heavily on macroscale surveys and bulk geochemical analyses (Liu et al., 2009; Jiang, 2008; Pedley, 2010). While these approaches effectively capture large - scale deposition patterns and system - level evolution, they often overlook the role of localized carbonate particles critical for understanding fine - scale geomorphic and biogeochemical processes. Thus, this study employs a multiscale, interdisciplinary methodology integrating: microscopic petrography to characterize particle morphology, internal structures, and microbial associations; in - situ hydrochemical testing to link particle formation to dynamic environmental conditions; and molecular biological techniques to elucidate biotic - abiotic interactions. By applying this framework, the study identifies specific sedimentary environments and conditions, explores the factors controlling carbonate particle deposition. Highlighting travertine deposition complexity, this work contributes to carbonate sedimentation knowledge, provides a framework for studying mineralogical - geochemical - biological interactions in continental settings. Significantly, it offers practical implications for environmental monitoring and conservation in regions with delicate karst landscapes, where understanding carbonate deposition is crucial for preserving these unique natural resources.

2 Materials and methods

2.1 Study area and sample collection

2.1.1 Study area

The Huanglong Scenic Area, located in the northern part of Songpan County, Aba Tibetan and Qiang Autonomous Prefecture, Sichuan (China) lies within the southern Minshan Mountains, where the Qinghai-Tibet Plateau transitions into the Sichuan Basin (Figures 1a,b). The region features alpine canyon terrain, with slopes ranging from southwest to northeast. The Huanglong Scenic Area spans 38 km north-south and 23 km east-west, with an elevation range of 1700–5588 m. Due to its unique geographical position, the area experiences a cold and arid monsoon climate, characteristic

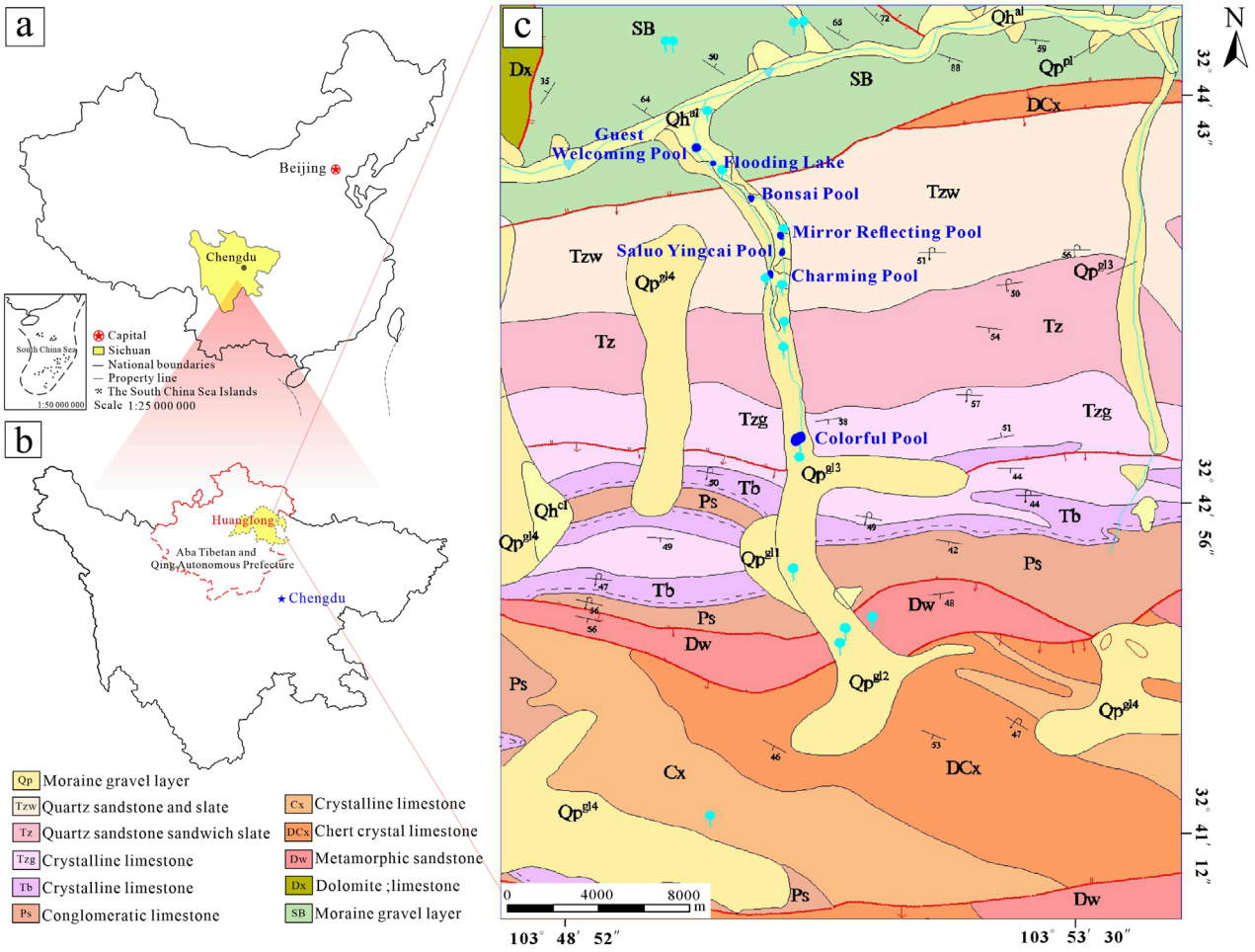

FIGURE 1
Study the geographical location and geological structure of the area. **(a)** Geographical location of Sichuan. **(b)** Geographical location of the Huanglong study area. **(c)** Structural and geological map of the Huanglong study area.

of the plateau temperate monsoon (Liu et al., 2003). The core area boasts a vibrant travertine landscape, including thousands of colorful pools, with Huanglong Ravine being the primary attraction (Figure 1c). The Huanglong Ravine is located at the confluence of three structural units: the Yangtze paraplatform, the Songpan-Garze fold system, and the Qinling fold system (Cao et al., 2009; Zhang et al., 2015). The outcropped rock formations in the Huanglong area date from the Silurian to Triassic periods, with a total thickness exceeding 2,700 m. The dominant lithologies are limestone, bioclastic limestone, and dolomite (Figure 1c). The southern margin of Wangxiangtai is predominantly Devonian, Carboniferous, and Permian limestone, dolomitic limestone, and bioclastic limestone, while the northern part mainly consists of Triassic sandstone, Silurian slate, and intercalated slate and limestone (Team, 2001).

Surface water from rainfall, snowmelt, and springs, particularly from the Zhuanhua Spring Group, serves as the primary water source for Huanglong Ravine. This constant water supply is crucial for travertine formation in the valley (Guo et al., 2002). The pH of surface water in the study area ranges from 6.81 to 8.62, with most waters showing alkaline characteristics. Hydrochemical analysis reveals that it falls in the category of HCO_3–Ca, with Ca^{2+} and Mg^{2+} as the principal cations and HCO_3^-as the dominant anion (Gao et al., 2023).

2.1.2 Sample Collection

These particles primarily gather along the gentle lower edges of rimstone dams within travertine pools. Similar deposits have been found in sloping flow systems near the Horseshoe Sea, Charming Pool, and Mirror Reflecting Pool (Figure 2). As a result, we chose four sites with notable particle accumulation - Colorful Pool, Horseshoe Sea, Charming Pool, and Mirror Reflecting Pool - as the sampling locations for the study. *In situ* sampling was carried out at these sites to examine the morphology and size variety of sand-like particles in the Huanglong area.

2.2 Analytical methods

To comprehensively characterize the carbonate particles in the travertine system and elucidate their formation mechanisms and

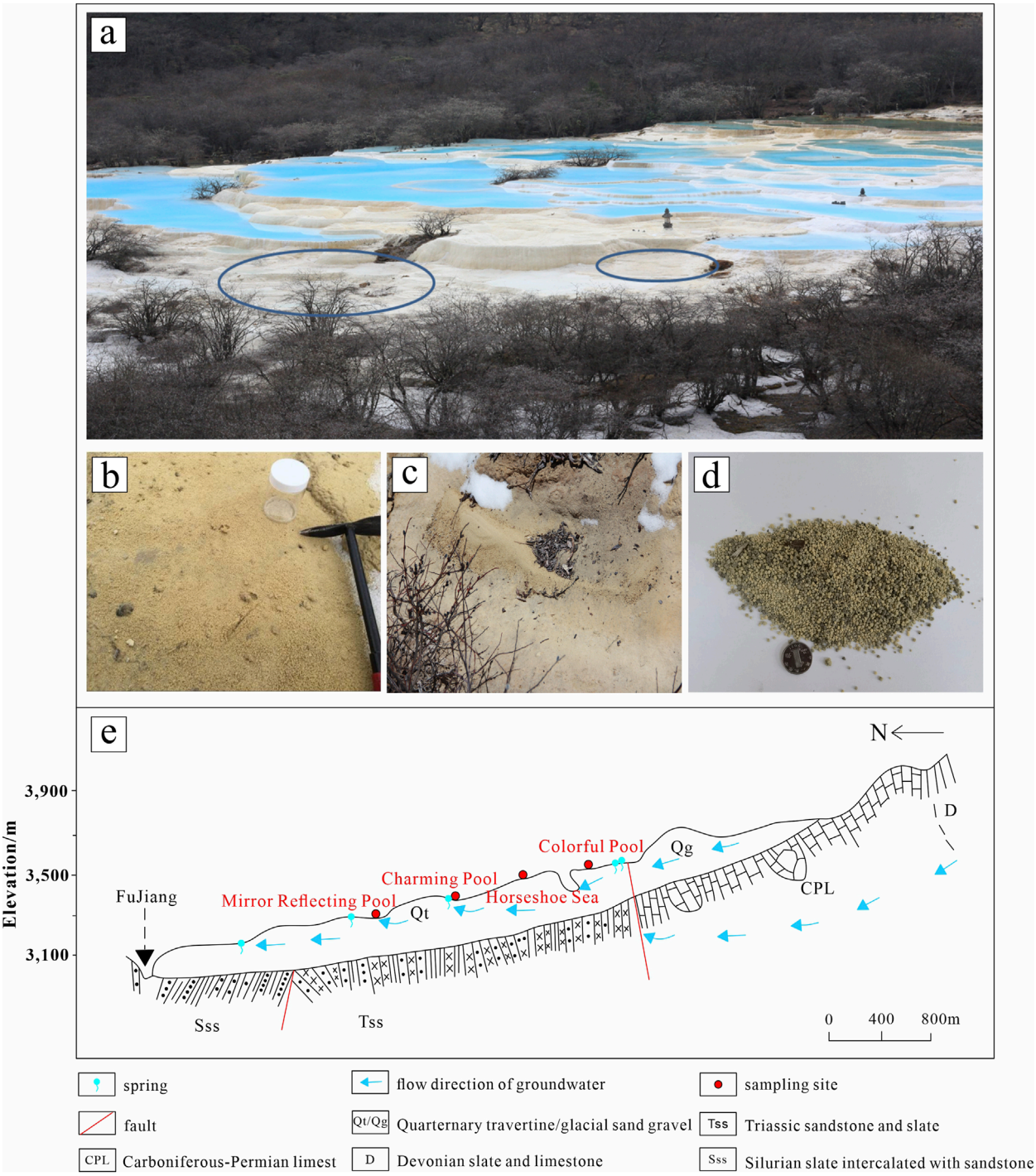

FIGURE 2
Map showing the sampling sites. **(a)** An overview of the multicolored pool, with the main accumulation areas of travertine particles circled in blue. **(b)** In the gentle area of the Horseshoe Sea, the particles are evenly distributed and conserved by water. **(c)** Field - observed accumulation morphology of particles. **(d)** Sample photograph. **(e)** Geological profile map and distribution of sampling points along Huanglong Ravine. Revised according to Liu et al. (1993).

environmental implications, a multi - faceted analytical approach was employed. This included hydrodynamic and hydrochemical analysis to understand the physical and chemical properties of the water environment, petrographic and mineralogical analysis encompassing petrography, scanning electron microscopy - energy dispersive spectroscopy (SEM - EDS), Tescan Integrated Mineral Analyzer (TIMA), and cathodoluminescence (CL) techniques (Table 1). These methods were systematically applied to examine particle morphology, mineral composition, elemental distribution, and growth characteristics, providing a holistic understanding of the travertine carbonate particles from multiple perspectives.

TABLE 1 Summary of analytical methods and technical parameters.

Analysis Type	Method/Instrument	Key Parameters	Target Characteristics
Hydrodynamic	Radarvelocimeter (HD-SCDPL)	Range: 0.1–30 m/s Accuracy: ±2% ± 0.03 m/s	Spatial flow variability
Hydrochemical	WTW Multi 3630 IDS Titration: VISOCOLOR® ECO/HE	pH: ±0.004 DO: ±0.5% Conductivity: ±0.5%	Ca^{2+}-HCO_3^- equilibrium Calcite saturation index
Petrographic	Polarizing microscope (Zeiss)	Thin-section: 30 μm Magnification: 50-200×	Grain morphology/cementation Growth zoning
Microanalysis	SEM-EDS (HITACHI SU8010)	Voltage: 0.3–30 kV Beam current: 1 pA-1 μA Detection limit: 0.1%–0.5%	Micromorphology/element distribution Organic matter occurrence
Automated Mineralogy	TIMA3X GMH	Resolution: 1 nm Beam current: 2 pA-200 nA	Quantitative mineralogy
Cathodoluminescence	GATAN MonoCL3+	Spatial resolution: ~10 μm Elements: Mn^{2+}/Fe^{2+}	Primary or secondary carbonate discrimination; Cementation sequence

Green rows = Fieldwork measurements; Blue rows = Laboratory analyses.

2.2.1 Hydrodynamic and hydrochemical analysis

Hydrodynamic tests were conducted at four sampling points, focusing on flow velocity. A portable radar wave velocity meter (HD-SCDPL, Surface Velocity Radar) using K-band radar was employed for non-contact flow velocity measurements (range: 0.1–30 m/s, accuracy: ±2% ± 0.03 m/s). Multiple measurements were averaged and recorded.

A WTW Multi 3630 IDS (Intelligent Digital Sensor) digital multiparameter analyzer with three IDS sensor ports was used to measure pH, oxidation-reduction potential (ORP), dissolved oxygen (DO), and conductivity/total dissolved solids (TDS)/salinity. The pH range was 0.00–14.00 (accuracy: ±0.004), DO ranged from 0.00 to 20.00 mg/L (accuracy: ±0.5%), and conductivity ranged from 10 μS/cm to 2000 μS/cm (accuracy: ±0.5%).

Water samples were collected using a syringe and filtered through a 0.45 μm membrane filter to remove particulate matter. Titrimetric test kits VISOCOLOR® ECO Calcium (1 drop = 5 mg/L Ca^{2+}) and VISOCOLOR® HE Alkalinity AL 7 (0.2–7.2 mmol/L OH^-) were used to measure Ca^{2+} and HCO_3^-concentrations. The calcite saturation index was determined using PHREEQC-I version 3.6.2.

2.2.2 Petrographic and mineralogical analysis

1. Petrography

Initial particle morphology was observed using a binocular microscope to characterize general morphology prior to detailed sectioning. For thin-section preparation, samples were systematically selected based on three criteria: representativeness of grain size; morphological integrity (excluding fractured or abraded particles), and diversity of surface textures. The selected samples were then prepared into standard 30 μm thin sections for detailed analysis under a polarizing microscope, enabling examination of particle morphology, crystallization patterns (including growth zoning), and internal cementation characteristics across different size fractions.

2. Scanning Electron Microscopy-Energy Dispersive Spectroscopy (SEM-EDS) Analysis

Samples showing complete particle structures were fixed in a 2% glutaraldehyde solution and stored in darkness for 2 days. They were air-dried and gold-coated to enhance conductivity. Microstructural analysis and organic content assessment were conducted using a HITACHI SU8010 SEM at Northwest University of China. Additionally, semi-quantitative analysis of sample elements was performed using EDS (X-MaxN 50). The detection limit ranged from 0.1% to 0.5%, with a beam current intensity of 1 pA to 1 μA, acceleration voltages ranging from 0.3 kv to 30 kv, and a working distance spanning from 5 mm to 80 mm. Sample sizes were tailored to thin slices with diameters of approximately 1–3 mm, based on particle size, and a combination of point and area analysis was employed to ensure representative coverage.

3. Tescan Integrated Mineral Analyzer (TIMA)

The Tescan Integrated Mineral Analyzer (TIMA3X GMH model, Northwest University, China) is an automated mineralogy system that combines scanning electron microscopy with energy-dispersive X-ray spectroscopy (SEM-EDS) for high-throughput mineralogical characterization. It can be specifically employed to: (1) quantitatively determine the modal mineralogy of sand-like particles, (2) map mineral associations at the micrometer scale, and (3) statistically analyze particle size distributions. The system offers a 1.0 nm resolution, with an acceleration voltage range from 200 V to 30 kV and an electron beam current range from 2 pA to 200 nA. Data from 20 samples were used to determine the mineral species, content, and distribution of the particles. These 20 samples were carefully selected from limited available materials due to protection restrictions in the Huanglong travertine scenic area, ensuring they

TABLE 2 Hydrochemical and hydrodynamic parameters of sampling points.

Parameters	Colorful pool	Horseshoe sea	Charming pool	Mirror reflecting pool
Flow velocity (m/s)	0.150	0.500	0.157	0.478
Temperature (℃)	10.9	12.9	12.4	11.7
pH	8.08	8.17	8.18	8.25
Conductivity (uS/cm)	951	630	652	657
Ca^{2+} (mM)	4.59	3.12	3.25	3.00
Alkalinity (mM)	10.0	6.6	6.8	6.8
Saturation index of calcite	1.442	1.263	1.299	1.313
pCO_2 (ppm)	4,627.00	2,623.01	2,568.62	2,133.04

Field measurements were conducted in September 2024 (autumn; air temp: 10 ℃–17 ℃).

are morphologically intact with fresh surfaces free from subsequent erosion.

4. Cathodoluminescence (CL)

The GATAN MonoCL3+ system at Northwest University was used in conjunction with scanning electron microscopy to examine growth zoning, microcracks, and alteration features in the samples. This technique detects trace-element variations (particularly Mn^{2+} and Fe^{2+} signatures) at ~10 μm spatial resolution, enabling identification of growth zonation patterns, diagenetic overprinting features, and cementation boundaries that are crucial for understanding travertine paragenesis but often indistinguishable through conventional microscopy. The CL imaging, performed in conjunction with scanning electron microscopy, reveals textural features including luminescence bands indicative of primary growth, Mn-activated luminescence or Fe-quenched zones characteristic of diagenetic alteration, and abrupt luminescence shifts marking cementation boundaries (Pagel et al., 2000; Götze and Kempe, 2008; Götze, 2012). While CL does not provide absolute trace-element concentrations, its high sensitivity to crystal chemistry variations makes it particularly valuable for differentiating genetic carbonate phases in our study of Huanglong travertines. All analyses followed the methodological framework of with instrument settings calibrated using standard calcite reference materials to ensure analytical consistency, as the technique's ability to simultaneously visualize both depositional structures and alteration features was essential for reconstructing the complex formation history of these carbonates.

3 Result

3.1 Depositional setting of sand-like particles

Modern, sand-like particles are actively forming in the small depressions between rimstone dams within travertine pools along Huanglong Ravine. Notable deposition sites include the Colorful Pool, Horseshoe Sea, Charming Pool, and Mirror Reflecting Pool. These depressions exhibit water depths of 1–5 cm, where particles deposition occurs. Flow velocities in these areas range from 0.150 m/s to 0.500 m/s, with average water temperatures of 11.9 C and an average pH of 8.17. The water temperature initially increases and subsequently decreases along the flow path from the Colorful Pool to the Mirror Reflecting Pool, despite the decreasing altitude. This phenomenon is attributed to the significant diurnal temperature variation in the Huanglong area. Specifically, when measuring the water temperature of the Mirror Reflecting Pool, the readings were taken near dusk when ambient air temperatures had decreased. Ca^{2+} concentrations range from 3.00 mM to 4.59 mM, alkalinity ranges from 6.6 mM to 10 mM, and the average pCO_2 is 2987.92 ppm (Table 2).

3.2 Composition

TIMA results demonstrate that 97.31% ± 1.25% of the particles' composition is calcite, with minor occurrences of quartz and anorthite (Table 3). Exogenous minerals such as mica, wollastonite, and ferro-actinolite are present within the interstitial spaces and growth suture lines, indicating a mix of endogenous and external influences during formation.

Energy-dispersive X-ray spectroscopy (EDS) identifies $CaCO_3$ as the primary component of the particles. In addition to C, O, and Ca, the particles also contained significant amounts of Fe, Si, K, Mg, Al (Table 4). Howe sand-like particles ver, spectra 3 and 7, which do not correspond to the particles, show significantly lower Ca content. At these points, elements like C, O, and Al dominate, likely due to the characteristics of the testing platform background.

3.3 Petrographic characteristics of sand-like particles

The sand-like particles exhibit predominantly spherical to sub-spherical shapes, with occasional elongated spheroids (Figure 3).

10.3389/feart.2025.1654910

TABLE 3 TIMA mineral composition statistics of sand-like particles.

Primary phases	1–1	1–2	1–3	1–4	2–1	2–2	2–3	2–4	3–1	3–2	3–3	3–4	4–1	4–2	4–3	4–4
Calcite	99.48	96.79	98.35	97.48	97.75	96.48	97.44	98.67	99.24	97.31	97.46	94.14	97.24	95.78	96.01	93.48
Quartz	0.06	0.42	0.16	0.16	0.45	0.21	0.17	0.16	0.16	0.49	0.22	0.39	0.25	0.32	0.03	0.18
Anorthite	0.16	0.24	0.14	0.15	0.37	0.22	0.15	0.12	0.18	0.31	0.18	0.10	0.22	0.18	0.12	0.31
Albite	0.02	0.06	0.00	0.01	0.12	0.04	0.06	0.00	0.02	0.09	0.02	0.04	0.04	0.05	0.01	0.01
Muscovite	0.01	0.05	0.02	0.02	0.03	0.06	0.01	0.01	0.01	0.04	0.00	0.04	0.02	0.03	0.00	0.00
Ferro-Actinolite	0.02	0.02	0.01	0.02	0.07	0.01	0.01	0.01	0.00	0.05	0.03	0.00	0.02	0.03	0.00	0.02
Wollastonite	0.00	0.03	0.01	0.03	0.04	0.01	0.02	0.00	0.00	0.01	0.02	0.00	0.01	0.00	0.00	0.00
Orthoclase	0.00	0.04	0.00	0.00	0.05	0.01	0.00	0.00	0.00	0.03	0.01	0.02	0.01	0.00	0.00	0.00
Hematite/ Magnetite	0.02	0.03	0.00	0.01	0.00	0.02	0.02	0.00	0.00	0.01	0.00	0.00	0.02	0.01	0.02	0.00
Diopside	0.00	0.01	0.00	0.01	0.00	0.00	0.00	0.00	0.00	0.00	0.00	0.00	0.00	0.00	0.01	0.06
Plagioclase	0.01	0.00	0.00	0.00	0.01	0.01	0.00	0.02	0.00	0.02	0.01	0.00	0.00	0.02	0.00	0.00
Ankerite	0.02	0.00	0.00	0.00	0.00	0.00	0.00	0.02	0.00	0.01	0.00	0.00	0.01	0.00	0.00	0.00
Garnet-Pyrope	0.00	0.00	0.00	0.02	0.01	0.00	0.00	0.00	0.00	0.00	0.00	0.00	0.00	0.00	0.00	0.00
Biotite	0.00	0.00	0.00	0.00	0.01	0.00	0.00	0.00	0.00	0.03	0.00	0.00	0.00	0.00	0.00	0.00
Titanite	0.00	0.00	0.00	0.00	0.00	0.00	0.00	0.00	0.00	0.00	0.00	0.00	0.02	0.00	0.00	0.00
Monazite	0.00	0.00	0.00	0.00	0.00	0.00	0.00	0.00	0.00	0.00	0.01	0.00	0.00	0.00	0.00	0.00
[Unclassified]	0.22	2.29	1.31	2.10	1.10	2.91	2.11	0.99	0.37	1.59	2.05	5.26	2.15	3.56	3.80	5.92
The rest	0.00	0.02	0.00	0.01	0.00	0.00	0.00	0.00	0.01	0.01	0.00	0.00	0.00	0.00	0.00	0.00
Total	100.0	100.0	100.0	100.0	100.0	100.0	100.0	100.0	100.0	100.0	100.0	100.0	100.0	100.0	100.0	100.0

Samples 1–1, 1–2, 1-3, and 1-4 were collected from Colorful Pool; samples 2–1, 2–2, 2-3, and 2-4 from Horseshoe Sea; samples 3–1, 3–2, 3-3, and 3-4 from Charming Pool; samples 4–1, 4–2, 4-3, and 4-4 from Mirror Reflecting Pool.

Their surfaces are irregularly rough, resembling aggregates of numerous minute fragments. Surface colors vary from yellow to light yellow, occasionally interspersed with black specks (Figure 3a). The particles are mechanically robust, resisting hand-crushing but yielding to knife cuts. Their sizes range from 0.5 mm to 3.0 mm, with some reaching up to 5 mm in long-axis diameter. Based solely on particle size, these deposits are a mixture of ooids and pisoids. Microscopic examination reveals the particle surfaces, characterized by irregular contours and protrusions (Figure 3b). These protrusions are calcite crystals displaying radial growth patterns (Figure 3c).

3.3.1 Internal structures and composition

At higher magnifications, the particles are composed primarily of calcite crystals of various shapes, including triangular and elongated rhombohedral forms (Figure 4a), as well as irregular polygonal detrital minerals that have just begun to gather and bond while maintaining distinct, uneroded edges and corners (Figure 4c), indicating they have not been significantly affected by flowing water or weathering processes. Unlike oolites, these particles lack distinct, single-material nuclei and instead exhibit a rough internal radial structure. Polarizing microscopy highlights distinct growth patterns and bonding characteristics of calcite crystals under plane polarized light, particularly showing how pseudo-triangular detrital materials gather at vertices to form relatively stable aggregation structures at initial nucleation points (Figure 4b).

Microscopic analyses differentiate the particles into two regions. The central region primarily consists of bonded clastic components. The peripheral region displays radial divergent growth (Figure 4c) contributing to irregular, convex shapes along the outer boundaries (Figure 4d). Discrepancies in clarity are observed at particle aggregation and bonding sites, indicating variations in their development stages.

10.3389/feart.2025.1654910

TABLE 4 EDS spectral spot measurements of the sand-like particles.

Spectrum	Element	Line type	Weight (%)	Weight sigma	Atomic (%)
Spectrum 1	C	K series	31.20	0.31	40.31
	O	K series	47.76	0.32	43.93
	Ca	K series	18.27	0.28	13.60
	Al	K series	2.07	0.11	1.57
	Si	K series	0.25	0.08	0.18
	Na	K series	0.45	0.13	0.40
Spectrum 2	C	K series	35.19	0.57	45.53
	O	K series	49.99	0.58	48.55
	Ca	K series	13.87	0.26	5.38
	Al	K series	0.95	0.08	0.55
Spectrum 3	C	K series	71.94	0.44	78.28
	O	K series	24.61	0.44	20.10
	Al	K series	2.59	0.07	1.26
	Ca	K series	0.30	0.04	0.10
	Si	K series	0.24	0.04	0.11
	Cl	K series	0.15	0.04	0.06
	Na	K series	0.17	0.05	0.10
Spectrum 4	C	K series	33.62	0.66	43.12
	O	K series	54.14	0.66	52.13
	Ca	K series	11.94	0.28	4.59
	Al	K series	0.30	0.08	0.17
Spectrum 5	C	K series	33.30	0.67	43.41
	O	K series	51.71	0.68	50.62
	Ca	K series	14.41	0.31	5.63
	Al	K series	0.58	0.09	0.34
Spectrum 6	C	K series	33.94	0.53	43.54
	O	K series	53.51	0.53	51.54
	Ca	K series	12.02	0.22	4.62
	Al	K series	0.53	0.07	0.30
Spectrum 7	C	K series	69.88	0.29	76.72
	O	K series	25.70	0.29	21.18
	Al	K series	3.30	0.05	1.61

(Continued on the following page)

TABLE 4 (*Continued*) EDS spectral spot measurements of the sand-like particles.

	Element	Line type	Weight (%)	Weight sigma	Atomic (%)
	Ca	K series	0.37	0.03	0.12
	Na	K series	0.28	0.03	0.16
	Cl	K series	0.25	0.02	0.09
	Si	K series	0.23	0.02	0.11

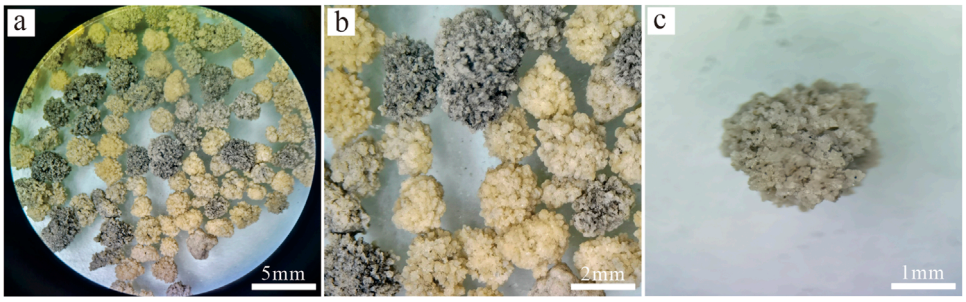

FIGURE 3
Morphological features of particles under the microscope **(a)** 2× microscope field of view. **(b)** 5× microscope field of view. **(c)** 10× local morphology under the microscope.

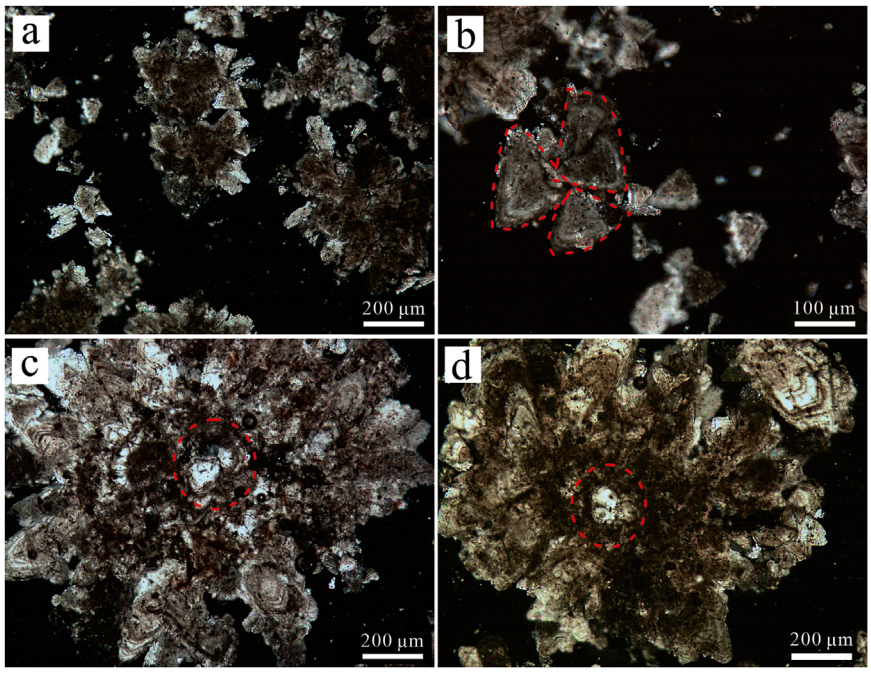

FIGURE 4
Particles morphology under microscope. **(a,b)** Particles morphology under a plane polarized. **(c,d)** Comparison between the inner central structure and the outer structure of the particle under a single polarizer.

3.3.2 Growth zoning and cementation

The internal structures and mineral crystallization characteristics of particles were observed under a single polarizer and a scanning electron microscope. Firstly, under a high - magnification microscope, a large number of growth zoning of calcite can be seen (Figures 5a,b), and there are three groups of

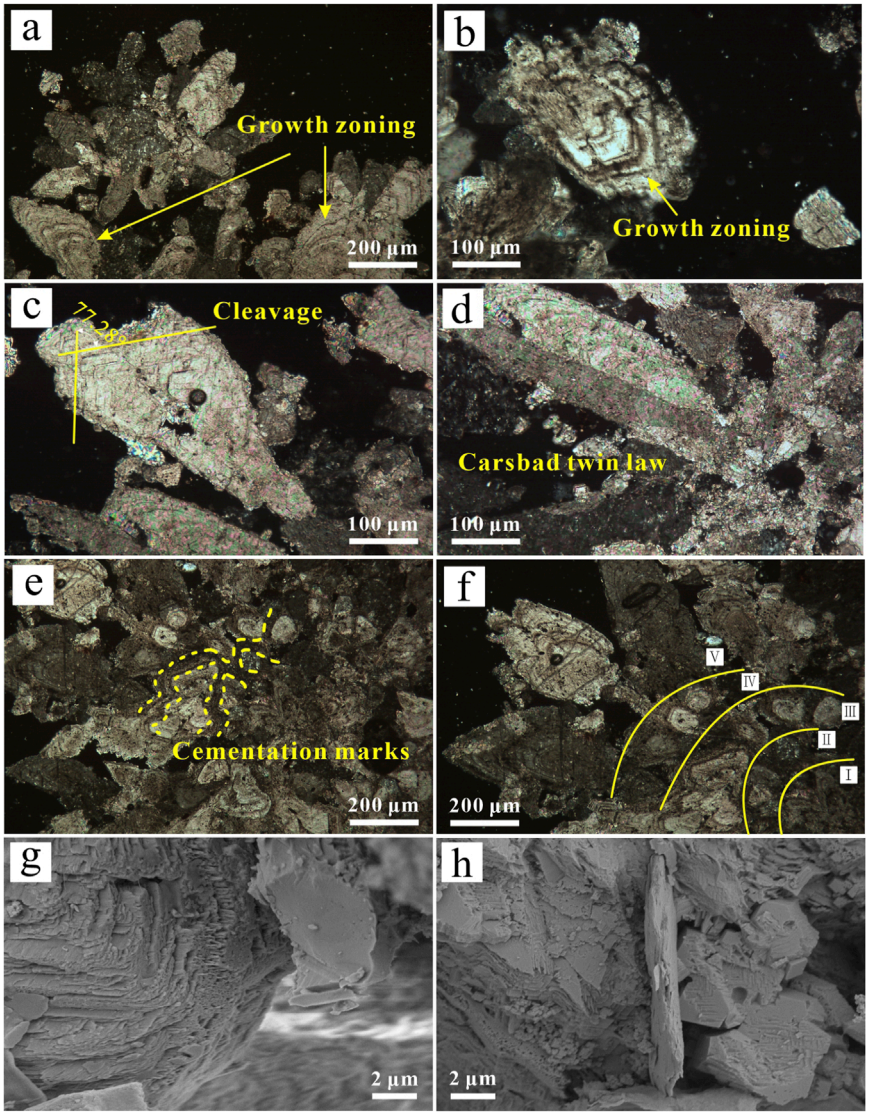

FIGURE 5
Characteristics of internal adhesion and mineral crystallization mode of particles. (a-f single polarizer, g-h scanning electron microscope). **(a)** The yellow dotted line indicates that during the growth of the particles, the calcite minerals are bonded together by microcrystalline matrix and sparry cement. **(b)** The particle may have gone through five growth stages so far. **(c,d)** Clear calcite growth rings. **(e)** Calcite shows 3 complete cleavage morphologies. **(f)** Carlsbad twin law - based dual crystal structure. **(g,h)** Calcite with good crystallization order, columnar growth, and layered development.

complete cleavage morphologies (Figure 5c). Some particles show twinning characteristics under cross - polarizers—one monomer undergoes extinction while the other remains bright, which is consistent with the Carlsbad twin law (Figure 5d). Cementation marks can be seen inside larger particles, and calcite minerals are bonded to each other by a microcrystalline matrix and sparry cement (Figure 5e). The interior of the particles is not completely dense; due to the insufficient fit of crystals of different shapes during aggregation, there are a large number of voids inside. These voids are filled with micritic and sparry cement, thus outlining the original particle boundaries. Evidence of multi - stage growth and cementation can be seen in mature particles, extending from the center to the periphery (Figure 5f), resulting in blurred boundaries of individual particles and their welding. In addition, calcite shows good crystallization order and mainly grows layer by layer in the form of columnar crystallization (Figures 5g,h).

3.4 Form of organisms in sand-like particles

Biological processes significantly influence the deposition of $CaCO_3$, with microbes playing a pivotal role through their growth and metabolic activity (Al-Qayim and Ghafor, 2022; Christos et al., 2022; Ghafor et al., 2012; Ghafor and Mohialdeen, 2016; Ghafor and Najaflo, 2022; Sharbazheri et al., 2009; Tri et al., 2023). Calcifying algae contribute structural frameworks for travertine deposition, while additional mechanisms such as product induction and metabolic regulation have also been identified (Jones and Renaut, 2010; Gradziński, 2010; Shiraishi et al., 2010).

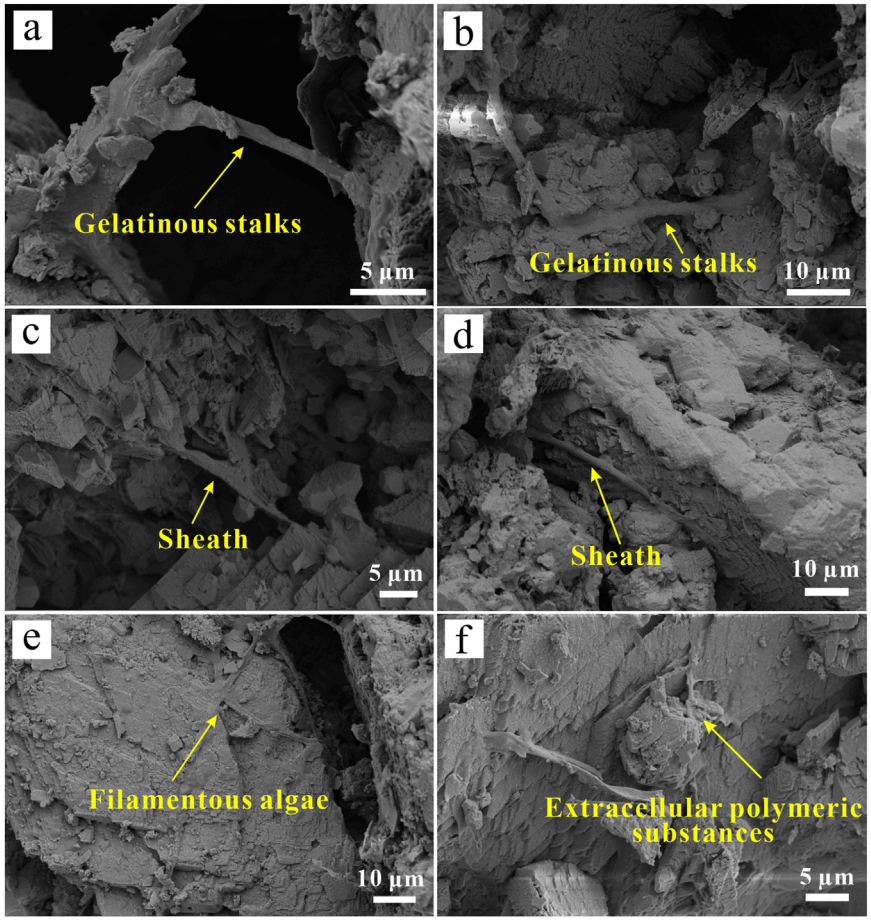

FIGURE 6
Biological traces involved in the formation process. **(a,b)** The gelatinous stalks of algae serve as a "template" for travertine deposition and play a connecting role. **(c,d)** Algal sheaths, around which calcite particles grows. **(e)** Filamentous algae interspersed among calcite crystals, forming complex and sparse structures. **(f)** Extracellular polymeric substances (EPS).

SEM reveals clear biological traces within the calcite crystal crevices, including algal filaments, gelatinous stalks (Figures 6a,b), and algal sheaths (Figures 6c,d), that connect calcite minerals at both ends of the crevices. Filamentous algae and their viscous secretions adhere to the surfaces of calcite crystals, promoting crystal growth. Radial crystalline growth is observed surrounding algae and their secretions, reinforcing their role in facilitating mineral deposition (Figures 6e,f).

3.5 Application of cathodoluminescence in particles

Cathodoluminescence provides a more precise method for analyzing the developmental stages of cement structures and pore-filling cement than traditional approaches such as tracing, staining, and optical microscopy (Meyer, 1974; Fairchild, 1983). In this study, most particles exhibited weak blue luminescence (Figure 7a). At a scale of 100 μm, particles present localized areas of relatively more intense blue luminescence (Figure 7b). The luminescence in carbonate minerals is primarily influenced by impurities, with Mn serving as the activator and Fe acting as the quencher (Machel and Burton, 1991). While calcite typically exhibits yellow-orange to red luminescence, the blue luminescence observed in this study may be attributed to lattice defects rather than elemental activators (Amieux, 1982). Additionally, Luminescence patterns revealed distinct boundaries between luminescent and non-luminescent regions, highlighting the contact zones between particles and intergranular calcite cement. These patterns suggest that larger particles formed through the aggregation of smaller particles and mineral debris, supporting a staged cementation process (Figure 7c). Microscopic observations revealed biological traces and early rock debris sand-like particles materials exhibiting high rounding among particles (Figures 7e,f).

4 Discussion

4.1 Characteristics and depositional conditions of the sand-like particles

The Huanglong travertine system, characterized by its distinctive terrace landscapes, including colorful pools, slopes, and steep cliffs, provides a unique environment for the formation of the

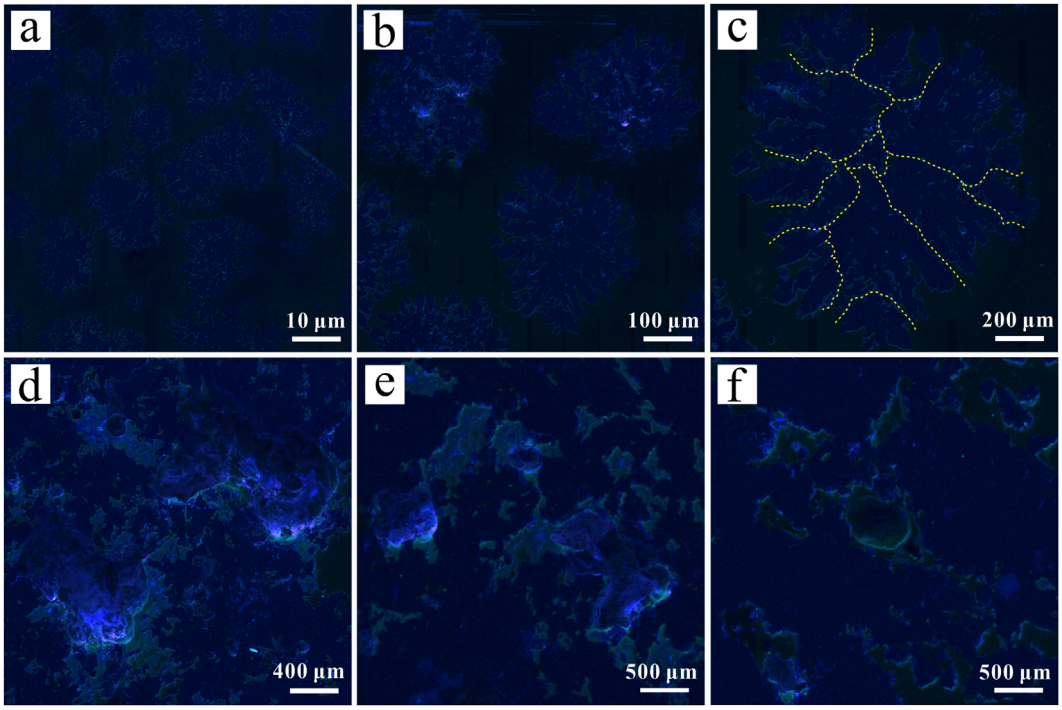

FIGURE 7
Cathodoluminescence characteristics of particles. **(a,b)** Overall blue glow of the particles. **(c)** The yellow dotted line shows the grain boundary, with more intense luminescence at the cementation points compared to the core of the calcite mineral. **(d)** The blue glow is intense with a slight purple glow. **(e)** Microscopic observation reveals that the biological surface also exhibits noticeable luminescence. **(f)** Early foreign inclusions at the particle bond, showing no luminescence.

particles. Therefore, these particles exhibit distinct morphological, structural, and depositional characteristics (Table 5).

The hydrodynamic conditions within Huanglong Ravine vary significantly, ranging from turbulent waterfalls to slow-flowing slopes, creating a dynamic setting that influences pisoid development. The particles predominantly accumulate in small depressions along the slope flow system, particularly in gentle areas near rimstone dams surrounding travertine pools. These areas represent transitional hydrodynamic conditions between turbulent and laminar flow, with velocities ranging from 0.150 m/s to 0.500 m/s, influenced by seasonal variations. During the rainy season, increased water flow transports particles over short distances, while the thin water layer flowing over the rimstone dams enhances the water-air interface, facilitating CO_2 escape and promoting rapid calcium carbonate deposition (Braithwaite, 1979; Dreybrodt and Buhmann, 1991; Jones and Peng, 2016; Schelker et al., 2016). In the dry season, decreased water flow leads to the drying of pools, halting sedimentation and exposing particles to air. This likely explains the blackened particles observed within the deposits, potentially caused by such as exposure - induced oxidation or organic staining by microbial communities (Li et al., 2011; Zhang et al., 2023).

Morphologically, the particles exhibit dendritic structures with rough, sub-spherical outer edges, lacking distinct concentric banding. Instead, they show radial growth. Elemental analysis reveals that the heightened Si content in the particles likely arises from both biological activity and the incorporation of quartz, feldspar, and mica debris transported by surface runoff during the rainy season (Liu et al., 2009). The presence of Fe, Mg, Al, and K further supports this hypothesis. Additionally, localized strong blue luminescence could result from high - temperature quartz or specific orientations of orthoclase, anorthite, and potassium feldspar (Figure 7b) (Zinkernagel, 1978).

Hydrochemically, the unique conditions in Huanglong, including a Ca^{2+} concentration of 4.59 mM, play a critical role in sand-like particles formation. These high concentrations, coupled with low-temperature calcium-rich waters sourced from cold springs and surface runoff, create an environment conducive to rapid calcite deposition. The interplay of biological activity and inorganic chemical deposition is critical, with seasonal changes significantly influencing sedimentation processes and resulting in the unique morphological and structural characteristics of the particles (Liu et al., 1995). In summary, these particles develop under transitional hydrodynamic conditions, where both organic and inorganic processes interact with seasonal precipitation to shape their formation, highlighting the importance of high Ca^{2+} concentrations, low hydrodynamic conditions, and seasonal variations in water flow.

4.2 Genesis model of travertine sand-like particles

The genesis of travertine sand-like particles can be attributed to two main processes: first, the formation of submillimeter-scale detritus or loose deposits through weathering, erosion, or denudation of pre-existing geomorphological features; and second,

TABLE 5 Characteristics of the sand-like particles.

Properties	The sand-like particles
Sedimentary environment	In the gentle area around the rimstone dams with slow flow velocity and laminar flow,v = 0.32 m/s
Shape	Sub-spheroidal, with irregular surface
Colour	Yellow and light yellow
Size	0.5 mm–3.0 mm, occasionally reaching up to 5 mm in long axis diameter
Mesoscopic structure	Roughly radial, without concentric rings and nucleus
Microscopic structure	The detrital particles are cemented by sparite and micritic cement, accompanied by the accretion of calcite
Mineralogy	Mainly calcite, but also contains quartz, feldspar and very small amounts of mica
Micro-organisms and organic matter content	Contains diatoms, filamentous algae and organic matter
Geochemistry	In addition to the high content of C, O and Ca, it also contains elements such as Fe, Si, K, Mg, Al
Hydrochemistry	T (℃) = 11.9, pH = 8.17, Alk (mM) = 7.55, Ca^{2+} (mM) = 4.59

the rapid crystallization of fine, submillimeter-sized calcite particles (Figure 4). In addition to calcite, the mineral composition includes exogenous materials such as quartz, feldspar, and mica, which are likely introduced from the surrounding terrain (Table 4). These materials are transported into the travertine system by flowing water following the denudation of nearby mountainous terrain.

The formation of these particles involves a process of "aggregation-cementation-accretion-compaction" of travertine clasts, exogenous debris, and calcite particles (Witten and Sander, 1981; Meakin, 1983; Jullien and Kolb, 1984). Based on field observations of sand-like particle accumulation (Figure 8a) and experimental results, a sedimentary model for the particles has been proposed (Figure 8). This model emphasizes the multifactorial nature of the sedimentation process.

Under favorable hydrodynamic conditions, detrital particles tend to agglomerate (stick together) and converge. In aquatic environments, four key forces act on particles:Effective gravity (W):Pulls particles downward; Horizontal shear force (Px):Pushes particles along the water flow direction; Vertical lift force (Pz):Lifts particles upward (reducing their weight in water); Resistance force (F):Slows particle movement (opposing Px/Pz). Px and Pz drive particles to move, while W and F act as counterforces (Figure 8c) (Liu et al., 2019). When slope flow hits debris/particles, a "push" on the upstream side causes upward + forward movement (Figure 8b). Meanwhile, eddies downstream create a pressure difference—like a "suction" that pulls particles forward gradually (Figure 8c) (Guha, 2008). Water currents combine Px (forward push) and Pz (upward lift) (Tai et al., 2020). Shear stress, turbulence, and differences in settling speed make particles bump into each other. Brownian motion (random particle jiggling) and weak forces from water films (bonding/van der Waals forces) help particles stick together (Zaichik et al., 2009).

Following agglomeration, as hydrodynamic conditions weaken, biological processes begin to influence $CaCO_3$ deposition. SEM imagery reveals the presence of organic entities, including diatoms, algal filaments, and extracellular polymers (Figure 6). Biological processes primarily impact travertine deposition through the following mechanisms (Figure 8f) (Wang et al., 2021):

Following agglomeration, as hydrodynamic conditions weaken, biological processes begin to influence $CaCO_3$ deposition. SEM imagery reveals the presence of organic entities, including diatoms, algal filaments, and extracellular polymers (Figure 6). Biological processes primarily impact travertine deposition through three key mechanisms (Figure 8f) (Wang et al., 2021):

1. Biological Assimilation–pH modulation via photosynthesis

Photosynthesis and respiration by aquatic flora induce changes in water pH, thereby influencing $CaCO_3$ precipitation (Merz-Preiß and Riding, 1999; Murray, 2003). During photosynthesis, algae release hydrogen ions (H^+), raising the pH of the water. This higher pH enhances the bonding between carbonate and calcium ions, increasing the $CaCO_3$ saturation coefficient and facilitating supersaturation and precipitation.

2. Biological Structure Role–algae as scaffolds for $CaCO_3$ precipitation

Algae act as both a matrix and scaffold for $CaCO_3$ deposition. In addition to photosynthesis, calcifying algae precipitate $CaCO_3$ through physiological and ecological processes, providing a structural framework (Figures 6a,b) (Dupraz and Visscher, 2005; Dupraz et al., 2008). Filamentous algae and their secretions also influence the morphology of calcium carbonate precipitates (Figures 6e,f).

3. Adhesion Mechanism–EPS promoting particle aggregation

Algae promote the formation of carbonate particles by binding micrite calcite and quartz particles (Schneider, 1977; Schneider et al., 1983; Gomez et al., 2018). In high Ca^{2+} environments, extracellular polymeric substances (EPS) adsorb Ca^{2+} ions, promoting calcification (Wright et al., 1996). Settling detrital particles become bound by algae and other organisms, undergoing calcification through metabolic processes (Pentecost, 1995; Wu et al., 2014). Calcite particles can grow along microbial sheaths (Figures 6c,d).

While travertine structures formed solely through biological processes tend to be loose, poorly compacted, and vulnerable to weathering, the particles exhibit strength and resist manual crushing. This observation suggests that inorganic processes also play a role in their formation. Polarized light microscopy reveals distinct calcite growth zoning structures, appearing as alternating bright and dark bands on calcite minerals (Figures 5c,d). SEM examination further reveals a crystalline order within the calcite particles in the aggregates (Figures 5g,h). These findings underscore

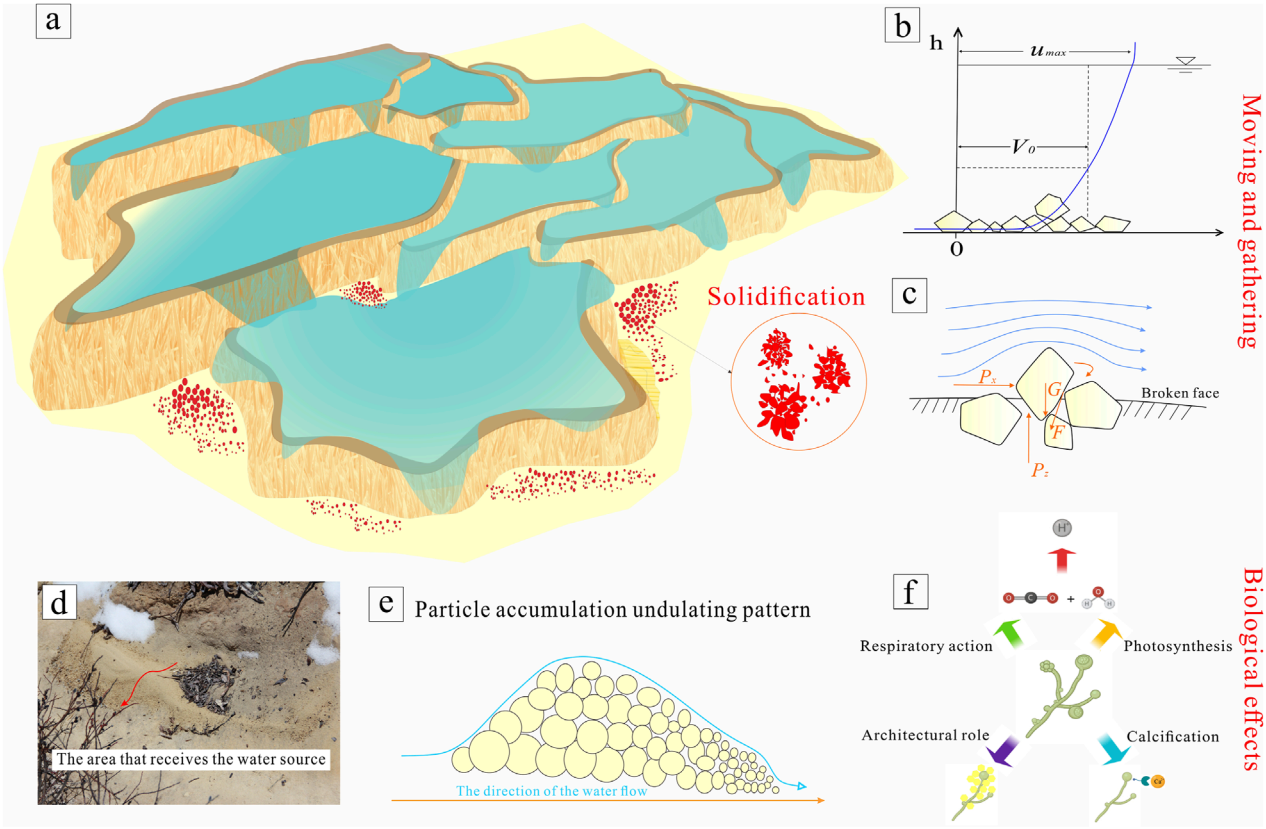

FIGURE 8
Schematic diagram of the sedimentation environment and process for sand-like particles. **(a)** Roughly illustrates a travertine pool system, with red markings representing where particles are typically deposited. **(b)** The movement of particle debris in the water stream. **(c)** Force analysis of detrital particles in water. **(d)** The particles are often accumulated in the receiving area of water release, and the accumulation situation is mostly similar to the undulation shown in **(e)**, the particles are affected by their own gravity, and the smaller the particles are more likely to be carried by the water flow to a slightly farther position. **(f)** Pathways of influence of biological processes on particle formation.

that the formation of the particles depends not only on microbial activity but also on the "accretion" of calcite. This accretion process, facilitated by algae, occurs along the boundaries of travertine detrital particles, resulting in pronounced growth and crystallization. The development of well-defined columnar crystals reduces void spaces between particles, thereby enhancing the consolidation and hardness of the aggregates.

The formation of travertine sand-like particles constitutes a complex process resulting from dynamic interactions between abiotic and biotic factors, characterized by multistage growth influenced by environmental conditions. Larger particles form through aggregation of smaller particles and mineral debris, supporting a staged cementation process. CL patterns reveal this progression: initial weak blue luminescence likely corresponds to early diagenetic phases with simple impurity incorporation, while more intense luminescence relates to later stages involving complex reactions and impurity enrichment. The observed particle boundaries and assemblages provide clear evidence for this growth and cementation sequence. Variations in cementation timing and degree result in differential interparticle void spaces. Furthermore, accretion and compaction processes progressively obscure individual calcite crystals near aggregate centers. The unique depositional environment of Huanglong facilitates initial development of small-scale microtopographic undulations (Figure 8d), with finer particles accumulating along flow directions (Figure 8e). Critically, seasonal precipitation affects particle growth by altering hydrodynamics, regulating hydrochemistry, and controlling biological activity. This climatic periodicity influences the distinct multi-stage growth patterns evident in both microscopic observations and CL analyses. However, more testing and detection matching work are still needed to clarify the specific control and regulation mechanisms.

4.3 The role of sand-like particles in the sedimentary evolution of Huanglong travertine landscape

The depositional evolution of different travertine landform types exhibits synergistic characteristics (Zhang et al., 2012a), with a positive feedback loop existing between particle deposition and microtopographic evolution. Taking travertine pools as an example, their life cycle encompasses the complete process from formation and development to eventual decline: During the pool

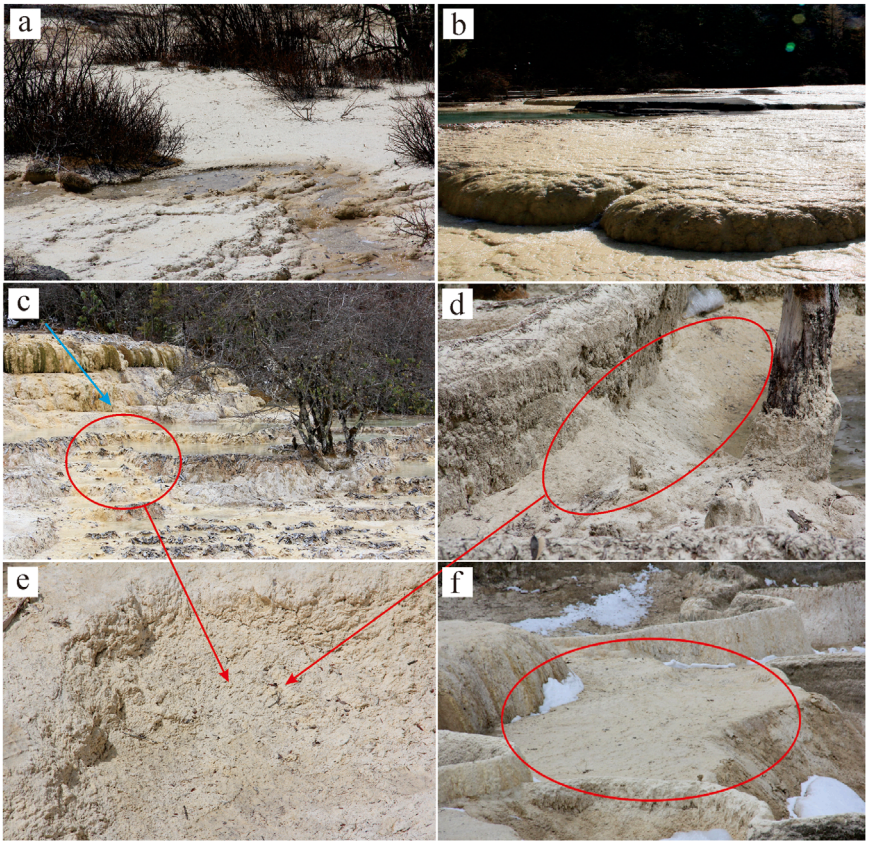

FIGURE 9
Sedimentary evolution of Huanglong travertine landscape influenced by sand-like particles. **(a)** Travertine slope affected by the particles. **(b)** Nascent travertine that are not covered by the particles. **(c)** Particles and debris are transported from top to bottom by the water flow for short distances, accumulating at similar locations in **(d)** and **(e)** and gradually increasing in size until the entire pot is filled. **(f)** Fill the travertine Colourful Pools with particles until it disappears.

formation stage, when particle-laden water overflows the dam, abrupt topographic changes cause kinetic energy attenuation, resulting in preferential deposition of coarse particles (with high inertia) at the dam crest while fine particles (such as micritic calcite) spread evenly across the pool bottom (Pedley, 1990). This differential deposition promotes continuous vertical growth and lateral expansion of rimstone dams. However, for mature travertine pools (e.g., abandoned pools in Yellowstone's Mammoth Hot Springs), their vertical sequences display coarse travertine debris from high-energy environments at the base, gradually transitioning upward to fine-grained travertine containing plant debris, and capped by alluvial sand layers at the top (Fouke, 2011).

Field observations in Huanglong reveal distinct depositional differentiation phenomena in travertine dams during flood seasons (May-September; Figures 9a,b). The thickness of newly formed travertine layers in sandy particle accumulation areas is significantly smaller than that of exposed travertine bodies, with some dams even exhibiting growth stagnation. In contrast, the dry season is dominated by weathering and erosion of secondary travertine. Erosion products from travertine surfaces form detrital particles that, when hydraulic conditions permit, are either transported short distances to flat areas (Figure 9c) or intercepted and retained by surface litter. Comparative analysis demonstrates that secondary travertine bodies covered by detrital particles are more susceptible to erosion. Notably, under the combined action of flowing water and wind, particles around dams undergo continuous migration-deposition cycles, with this dynamic process further amplifying their negative effects on dam structures. It can thus be inferred that particle deposition around travertine dams not only inhibits vertical accretion but may also compromise structural stability. Furthermore, particle cementation and filling alter the internal hydraulic conductivity of dams, leading to degradation of their original water retention capacity. With Huanglong's well-developed travertine terrace system and mature colored pools, when water flows forward from inclined beaches, particles are transported to the lower edges of rimstone dams or into colored pools, causing siltation and even pool disappearance (Figure 9f), indicating that particle accumulation predominantly exerts negative effects at this stage.

The travertine depositional system exhibits distinct phasic and cyclical characteristics, with its evolution controlled by multiple factors including hydrodynamic forces, biological activity, and detrital particle supply. Therefore, both landscape conservation practices and academic research must adopt systemic thinking to holistically consider the dominant processes and their interactions across different evolutionary stages. For instance, addressing particle accumulation issues in mature travertine pools requires integrated

approaches combining hydrodynamic regulation and ecological restoration to delay landscape degradation. This understanding holds universal significance for the sustainable management of similar travertine landforms worldwide.

5 Conclusion

1. The sand-like particles in the Huanglong travertine system represent a unique granular carbonate facies characterized by subspherical morphology, yellowish coloration, radial microstructures. Their internal architecture reveals growth zonation with clasts and sub-particles bound by sparitic-micritic cement, along with preserved organic matter, supporting a hybrid genesis involving both inorganic precipitation and microbial mediation.
2. These particles form under specific hydrodynamic (0.15–0.50 m/s flow velocities) and hydrochemical (Ca^{2+} = 4.59 mM) conditions along rimstone dam peripheries, where low-energy deposition dominates in response to seasonal hydrological fluctuations. Material sources include both detrital particles (weathering products) and authigenic calcite (rapid crystallization). The sedimentation process involves the "aggregation–cementation–accretion - compaction" of these sub-particles, driven by a combination of inorganic and organic factors, and is regulated by hydrodynamic and hydrochemical variations.
3. The sand-like particles play a stage-specific role in the sedimentary evolution of travertine landscapes, but currently exert predominantly negative impacts on the Huanglong travertine system, primarily manifested as: (i) These particles accumulate around travertine rimstone dams, altering the flow direction of water, and inhibiting the formation of new rimstone structures; (ii) Loose particles covering the surface of travertine terraces increase the permeability of the travertine, indirectly lowering the water table and increasing susceptibility to surface darkening and weathering; (iii) The significant generation and accumulation of these particles can fill travertine Colourful Pools, disrupting the landscape of travertine Colourful Pools.

Our findings underscore the unique depositional dynamics of sand-like particles in high Ca^{2+} spring systems and emphasize their role as sensitive indicators of hydrochemical and ecological change. The particles' distinct characteristics and sensitive microenvironmental records further validate their value for environmental and climatic change studies. Future studies could apply high-resolution time-series imaging to track seasonal particle growth dynamics, and integrate stable isotope analysis to disentangle inorganic precipitation pathways from microbial mediation processes.

Data availability statement

The original contributions presented in the study are included in the article/supplementary material, further inquiries can be directed to the corresponding author.

Author contributions

WH: Visualization, Writing – review and editing, Writing – original draft, Investigation. FW: Writing – review and editing, Funding acquisition, Methodology, Project administration. CP-M: Supervision, Writing – review and editing, Validation. EC: Methodology, Writing – review and editing, Conceptualization. SC: Visualization, Writing – review and editing. YW: Writing – review and editing, Software. YZ: Writing – review and editing, Formal Analysis. XZ: Supervision, Writing – review and editing. FD: Writing – review and editing, Formal Analysis. QZ: Resources, Writing – review and editing. XL: Writing – review and editing, Resources.

Funding

The author(s) declare that financial support was received for the research and/or publication of this article. This work was supported by the National Natural Science Foundation of China (grant no.41973053); the Opening Fund of the State Key Laboratory of Environmental Geochemistry (SKLEG2024221); the Open Fund of Guangxi Key Science and Technology Innovation Base on Karst Dynamics (grant no. KDLandGuangxi202302); the Open Fund of Key Laboratory of Mountain Disasters and Surface Processes of China Academy of Sciences (grant no. 19zd3105); the Open Fund of State Key Laboratory of Loess and Quaternary Geology, Institute of Earth Environment, Chinese Academy of Sciences (grant no. SKLLQG1620); The Project supported by graduate Innovation Fund of Southwest University of Science and Technology (24ycx1135); Sichuan Provincial Geological Exploration Project (DZ202318), Department of Natural Resources of Sichuan Province.

Acknowledgments

We are grateful for the financial support of the National Natural Science Foundation of China, the Huanglong National Scenic Spot Administration of Sichuan in China for their support in field investigation and sampling. Finally, we would like to thank the reviewers for their comments.

Conflict of interest

The authors declare that the research was conducted in the absence of any commercial or financial relationships that could be construed as a potential conflict of interest.

Generative AI statement

The author(s) declare that no Generative AI was used in the creation of this manuscript.

Any alternative text (alt text) provided alongside figures in this article has been generated by Frontiers with the support of artificial intelligence and reasonable efforts have been made to ensure accuracy, including review by the authors wherever possible. If you identify any issues, please contact us.

Publisher's note

References

Al-Qayim, B., and Ghafor, I. (2022). Biostratigraphy and paleoenvironments of benthic foraminifera from lower part of the damlouk member, western desert, Iraq. *Iraqi J. Sci.*, 4799–4817. doi:10.24996/ijs.2022.63.11.19

Amato, V., Anzalone, E., Aucelli, P. P. C., Argenio, B. D., Ferreri, V., and Rosskopf, C. M. (2012). Sedimentology and depositional history of the travertines outcropping in the Poseidonia-Paestum archaeological area. *Rendiconti Lincei* 23, 61–68. doi:10.1007/s12210-011-0155-z

Amieux, P. (1982). Cathodoluminescence: method of sedimentological study in carbonates. *Bull. Cent. Rech. Explor. Prod. Elf-Aquitaine*. 6, 437–483.

Braithwaite, C. J. R. (1979). Crystal textures of Recent fluvial pisolites and laminated crystalline crusts in Dyfed, South Wales. *J. Sediment. Res.* 49, 181–193.

Cao, J., Guo, J., and Yang, G. (2009). Evolutionary trend of the Huanglong travertine in songpan. *Acta Geol. Sichuan* 29, 222–228.

Capezzuoli, E., Gandin, A., and Pedley, M. (2014). Decoding tufa and travertine (fresh water carbonates) in the sedimentary record: the state of the art. *Sedimentology* 61, 1–21. doi:10.1111/sed.12075

Christos, K., Vasiliki, L., Artemis, P., Panagiotis, V., Ioannis, I., Maria, K., et al. (2022). Microbial mat stratification in travertine depositions of Greek hot springs and biomineralization processes. *Minerals* 12, 1408. doi:10.3390/min12111408

Croci, A., Porta, G. D., and Capezzuoli, E. (2016). Depositional architecture of a mixed travertine-terrigenous system in a fault-controlled continental extensional basin (Messinian, Southern Tuscany, Central Italy). *Sediment. Geol.* 332, 13–39. doi:10.1016/j.sedgeo.2015.11.007

Dong, F., Dai, Q., Jiang, Z., Chen, X., Xu, R., Zhang, Q., et al. (2023). Travertine/tufa resource conservation and sustainable development call for a world-wide initiative. *Appl. Geochem.* 148, 105505–5. doi:10.1016/j.apgeochem.2022.105505

Dreybrodt, W., and Buhmann, D. (1991). A mass transfer model for dissolution and precipitation of calcite from solutions in turbulent motion. *Chem. Geol.* 90, 107–122. doi:10.1016/0009-2541(91)90037-r

Dupraz, C., and Visscher, P. T. (2005). Microbial lithification in marine stromatolites and hypersaline mats. *Trends Microbiol.* 13, 429–438. doi:10.1016/j.tim.2005.07.008

Dupraz, C., Reid, R. P., Braissant, O., Decho, A. W., Norman, R. S., and Visscher, P. T. (2008). Processes of carbonate precipitation in modern microbial mats. *Earth-Science Rev.* 96, 141–162. doi:10.1016/j.earscirev.2008.10.005

Fairchild, I. J. (1983). Chemical controls of cathodoluminescence of natural dolomites and calcites: new data and review. *Sedimentology* 30, 579–583. doi:10.1111/j.1365-3091.1983.tb00695.x

Folk, R. L., and Chafetz, H. S. (1983). "Pisoliths (pisoids) in quaternary travertines of tivoli, Italy," in *Coated grains*. Editor T. M. Peryt (Berlin: Springer), 474–487.

Ford, T. D., and Pedley, H. M. (1996). A review of tufa and travertine deposits of the world. *Earth-Science Rev.* 41, 117–175. doi:10.1016/s0012-8252(96)00030-x

Fouke, B. W. (2011). Hot-spring systems geobiology: abiotic and biotic influences on travertine formation at Mammoth hot springs, Yellowstone national park, USA. *Sedimentology* 58, 170–219. doi:10.1111/j.1365-3091.2010.01209.x

Gao, J., Zhou, X., Fang, B., Li, T., and Tang, L. (2013). U-series dating of the travertine depositing near the Rongma hot springs in northern Tibet, China, and its paleoclimatic implication. *Quat. Int.* 298, 98–106. doi:10.1016/j.quaint.2012.08.003

Gao, W., Zhang, J., Zhang, W., Sun, D., Guo, J., Zhao, S., et al. (2023). Hydrochemical characteristics and driving factors of travertine deposition in Huanglong, Sichuan, SW. *China. Water Sci. Technol.* 875, 1232–1249. doi:10.2166/wst.2023.269

Garnett, E. R., Andrews, J. E., Preece, R. C., and Dennis, P. F. (2004). Climatic change recorded by stable isotopes and trace elements in a British Holocene tufa. *J. Quat. Sci.* 19, 251–262. doi:10.1002/jqs.842

Ghafor, I. M., and Mohialdeen, I. M. (2016). Fossils distribution from garagu formation (early cretaceous), diversity and paleoenvironmental conditions, kurdistan region, north Iraq. *Sulaimani J. Pure Appl. Sci.* 1, 139–149. doi:10.25271/2016.1.1.280

Ghafor, I. M., and Najaflo, S. (2022). Biostratigraphy, microfacies, paleoenvironment, and paleoecological study of the oligocene (late rupelian–early chattian) baba formation, kirkuk area, northeastern Iraq. *Carbonates Evaporites* 37, 7. doi:10.1007/s13146-021-00753-2

Ghafor, I. M., Karim, K. H., and Baziany, M. M. (2012). Age determination and origin of crenulated limestone in the eastern part of Sulaimaiyah Governorate, Kurdistan Region, NE-Iraq. *Iraqi Bull. Geol. Min.* 8, 21–30. doi:10.31257/ibgm.2012.08.01.03

Gomez, F. J., Mlewski, C., Boidi, F. J., Farías, M. E., and Gérard, E. (2018). Calcium carbonate precipitation in diatom-rich microbial mats: the Laguna Negra hypersaline lake, Catamarca, Argentina. *J. Sediment. Res.* 88, 727–742. doi:10.2110/jsr.2018.37

Götze, J. (2012). Application of cathodoluminescence microscopy and spectroscopy in geosciences. *Microsc. Microanal.* 18, 1270–1284. doi:10.1017/s1431927612001122

Götze, J., and Kempe, U. (2008). A comparison of optical microscope- and scanning electron microscope-based cathodoluminescence (CL) imaging and spectroscopy applied to geosciences. *Mineral. Mag.* 72, 909–924. doi:10.1180/minmag.2008.072.4.909

Gradziński, M. (2010). Factors controlling growth of modern tufa: results of a field experiment, 336. London: Geological Society, Special Publication, 143–191.

Guha, A. (2008). Transport and deposition of particles in turbulent and laminar flow. *Annu. Rev. Fluid Mech.* 40, 311–341. doi:10.1146/annurev.fluid.40.111406.102220

Guo, J. (2005). On protection of travertine landscape in the jiuzhai valleyand Huanglong scenic spots. *Acta Geol. Sichuan* 1, 23–26.

Guo, J., Peng, D., and Yang, J. (2002). A study of water circulation and genesis of travertine landscape in Huanglong. *Acta Geol. Sichuan* 1, 21–26.

Henchiri, M., Ahmed, W. B., Brogi, A., Alçiçek, M. C., and Benassi, R. (2017). Evolution of Pleistocene travertine depositional system from terraced slope to fissure-ridge in a mixed travertine-alluvial succession (Jebel El Mida, Gafsa, southern Tunisia). *Geodin. Acta* 29, 20–41. doi:10.1080/09853111.2016.1265398

Jiang, Z. (2008). A study of the formation and evolution trend of the Huanglong travertine landscape. *Hydrogeology Eng. Geol.* 1, 107–111.

Jones, B., and Peng, X. (2016). Mineralogical, crystallographic, and isotopic constraints on the precipitation of aragonite and calcite at Shiqiang and other hot springs in Yunnan Province, China. *Sediment. Geol.* 345, 103–125. doi:10.1016/j.sedgeo.2016.09.007

Jones, B., and Renaut, R. W. (2010). "Chapter 4 Calcareous Spring deposits in continental settings," in *Developments in sedimentology*. Editors A. M. Alonso-Zarza, and L. H. Tanner (Amsterdam: Elsevier), 177–224.

Jullien, R., and Kolb, M. (1984). Hierarchical model for chemically limited cluster-cluster aggregation. *J. Phys. A Math. General.* 17, 639–643. doi:10.1088/0305-4470/17/12/003

Kano, A., Okumura, T., Takashima, C., and Shiraishi, F. (2019). "Sedimentology of travertine," in *Geomicrobiological properties and processes of travertine: with a focus on Japanese sites*. Editors A. Kano, T. Okumura, C. Takashima, and F. Shiraishi (Cham: Springer), 43–66.

Li, Y., Tian, Y., and Li, Y. (2011). Tufa algae and biological karstification at Huanglong, Sichuan. *Carsologica Sin.* 30, 86–92.

Liu, Z. (2014). Research progress in paleoclimatic interpretations of tufa and travertine. *Chin. Sci. Bull.* 59, 2229–2239. doi:10.1360/n972013-00037

Liu, Z., Yuan, D., Dreybrodt, W., and Svensson, U. (1993). The formation of tufa in Huanglong, Sichuan. *Carsologica Sin.* 3, 185–191.

Liu, Z., Svensson, U., Dreybrodt, W., Yuan, D., and Buhmann, D. (1995). Hydrodynamic control of inorganic calcite precipitation in Huanglong Ravine, China: field measurements and theoretical prediction of deposition rates. *Geochimica Cosmochimica Acta* 59, 3087–3097. doi:10.1016/0016-7037(95)00198-9

Liu, Z., Yuan, D., He, S., Cao, J., You, S., Dreybrodt, W., et al. (2003). Origin and forming mechanisms of travertine at Huanglong ravine of sichuan. *Geochimica* 32, 1–10.

Liu, Z., Tian, Y., An, D., Wang, H., Zhang, J., Sun, H., et al. (2009). Formation and evolution of the travertine landscape at Huanglong, Sichuan, one of the world natural heritages. *Acta Geosci. Sin.* 30, 841–847. doi:10.3321/j.issn:1006-3021.2009.06.017

Liu, H., Zhang, J., Xiao, H., and Xie, C. (2019). Movement analysis of solid particles during the formation of swirl field. *Chem. Industry Eng. Prog.* 38, 1236–1243. doi:10.16085/j.issn.1000-6613.2018-1558

Lu, G., and Li, X. (1992). A study on cold-water travertine surface depositional landforms in Huanglong scenic spot, Sichuan Province, 19. Chengdu: Journal of Chengdu University of Technology, 55–64.

Lu, G., Zheng, C., Donahoe, R. J., and Lyons, W. B. (2000). Controlling processes in a CaCO3 precipitating stream in Huanglong natural scenic district, sichuan, China. *J. Hydrology* 230, 34–54. doi:10.1016/s0022-1694(00)00171-2

Machel, H. G., and Burton, E. A. (1991). "Factors governing cathodoluminescence in calcite and dolomite, and their implications for studies of carbonate diagenesis," in *Luminescence microscopy and spectroscopy: qualitative and quantitative applications*.

Editors H. G. Machel, E. A. Burton, C. E. Barker, R. C. Burruss, O. C. Kopp, and H. Y. Colburn (Tulsa: SEPM), 37–57.

Matsuoka, J., Kano, A., Oba, T., Watanabe, T., and Seto, K. (2001). Seasonal variation of stable isotopic compositions recorded in a laminated tufa, SW Japan. *Earth Planet. Sci. Lett.* 192, 31–44. doi:10.1016/s0012-821x(01)00435-6

Meakin, P. (1983). Formation of fractal clusters and networks by irreversible diffusion-limited aggregation. *Phys. Rev. Lett.* 51, 1119–1122. doi:10.1103/physrevlett.51.1119

Melim, L., and Spilde, M. N. (2018). A New Unified Model For Cave Pearls: Insights from Cave Pearls in Carlsbad Cavern, New Mexico, U.s.a. *U.S.A. J. Sediment. Res.* 88, 344–364. doi:10.2110/jsr.2018.21

Melim, L. A., Lieschеidt, R., Northup, D. E., Spilde, M. N., Boston, P. J., and Queen, J. M. (2009). A biosignature suite from cave pool precipitates, Cottonwood Cave, New Mexico. *Astrobiology* 9, 907–917. doi:10.1089/ast.2009.0345

Merz-Preiß, M., and Riding, R. (1999). Cyanobacterial tufa calcification in two freshwater streams: ambient environment, chemical thresholds and biological processes. *Sediment. Geol.* 126, 103–124. doi:10.1016/s0037-0738(99)00035-4

Meyer, R. T. (1974). Flash photolysis and time-resolved mass spectrometry. III. Termolecular and surface recombinations of ground state iodine atoms. *J. Phys. Chem.* 78, 878–881. doi:10.1021/j100602a006

Mors, R. A., Gomez, F. J., Astini, R. A., Celestian, A. J., and Corsetti, F. A. (2022). Assessing the origin of pisoids within a travertine system in the border of Puna Plateau, Argentina. *Sedimentology* 69, 1252–1275. doi:10.1111/sed.12946

Murray, B. (2003). The roles of carbonic anhydrases in photosynthetic CO2 concentrating mechanisms. *Photosynth. Res.* 77, 83–94. doi:10.1023/a:1025821717773

Pagel, M., Barbin, V., Blanc, P., and Ohnenstetter, D. (2000). *Cathodoluminescence in geosciences*. Berlin, Heidelberg, New York: Springer.

Pedley, H. M. (1990). Classification and environmental models of cool freshwater tufas. *Sediment. Geol.* 68, 143–154. doi:10.1016/0037-0738(90)90124-c

Pedley, M. (2010). Tufas and travertines of the Mediterranean region: a testing ground for freshwater carbonate concepts and developments. *Sedimentology* 56, 221–246. doi:10.1111/j.1365-3091.2008.01012.x

Pentecost, A. (1995). The Quaternary travertine deposits of Europe and Asia Minor. *Quat. Sci. Rev.* 14, 1005–1028. doi:10.1016/0277-3791(95)00101-8

Pentecost, A. (2005). *Travertine*. Berlin: Springer.

Porta, G. D. (2015). "Carbonate build-ups in lacustrine, hydrothermal and fluvial settings: comparing depositional geometry, fabric types and geochemical signature," in *Microbial carbonates in space and time: implications for global exploration and production*. London: Geological Society, 17–68.

Qiu, S., Wang, F., Dong, F., Tian, F., Zhao, X., Dai, Q., et al. (2022). Sedimentary evolution of the Dawan travertines and their geological environmental significance, Huanglong, China. *Depositional Rec.* 8, 251–265. doi:10.1002/dep2.165

Rodríguez-Berriguete, Á., Alonso-Zarza, A. M., García, R. M., and Cabrera, M. C. (2018). Sedimentology and geochemistry of a human-induced tufa deposit: Implications for palaeoclimatic research. *Sedimentology* 65, 2253–2277. doi:10.1111/sed.12464

Schelker, J., Singer, G. A., Ulseth, A. J., Hengsberger, S., and Battin, T. J. (2016). CO2 evasion from a steep, high gradient stream network: importance of seasonal and diurnal variation in aquatic pCO2 and gas transfer. *Limnol. Oceanogr.* 61, 1826–1838. doi:10.1002/lno.10339

Schneider, J. (1977). "Carbonate construction and decomposition by epilithic and endolithic micro-organisms in salt and freshwater," in *Fossil algae*. Berlin: Springer, 248–260.

Schneider, J., Schröder, H. G., and Le Campion-Alsumard, T. (1983). "Algal micro-reefs-coated grains from freshwater environments," in *Coated grains*. Berlin: Springer, 284–298.

Sharbazheri, K., Ghafor, I., and Muhammed, Q. (2009). Biostratigraphy of the Cretaceous/Tertiary boundary in the Sirwan Valley (Sulaimani Region, Kurdistan, NE Iraq). *Geol. carpathica* 60, 381–396. doi:10.2478/v10096-009-0028-x

Shiraishi, F., Okumura, T., Takahashi, Y., and Kano, A. (2010). Influence of microbial photosynthesis on tufa stromatolite formation and ambient water chemistry, SW Japan. *Geochimica Cosmochimica Acta* 74, 5289–5304. doi:10.1016/j.gca.2010.06.025

Tai, C., Wang, S., and Narsimhan, V. (2020). Cross-stream migration of non-spherical particles in a second-order fluid - theories of particle dynamics in arbitrary quadratic flows. *J. Fluid Mech.* 895, A6. doi:10.1017/jfm.2020.300

Tchouatcha, M. S., Njoya, A., Ganno, S., Toyama, R., Ngouem, P. A., and Njiké Ngaha, P. R. (2016). Origin and paleoenvironment of Pleistocene–Holocene Travertine deposit from the Mbéré sedimentary sub-basin along the Central Cameroon shear zone: Insights from petrology and palynology and evidence for neotectonics. *J. Afr. Earth Sci.* 118, 24–34. doi:10.1016/j.jafrearsci.2016.01.031

Team, S. G. A. M. (2001). *Ecological geology map and report of Huanglong*. Beijing: Geological Publishing House.

Temiz, U., Koçak, İ., Öksüz, N., and Akbay, S. (2021). Significance of neotectonic and paleoclimatic Late Pleistocene-Holocene travertine and origins: Balkayası, Avanos-Nevsehir, Central Anatolia/Turkey. *Int. J. Earth Sci.* 110, 2157–2177. doi:10.1007/s00531-021-02065-1

Tri, H. N. N., Huong, H. N. P., Van, T. H., and Khanh, S. N. (2023). A study on the applicability of microbially induced calcium carbonate precipitation on soil-sand stabilization through the bio-cementation process. *IOP Conf. Ser. Earth Environ. Sci.* 1226, 1755–1226. doi:10.1088/1755-1315/1226/1/012026

Verrecchia, E. P., Freytet, P., Verrecchia, K. E., and Dumont, J. L. (1995). Spherulites in calcrete laminar crusts; biogenic CaCO3 precipitation as a major contributor to crust formation. *J. Sediment. Res.* 65, 690–700. doi:10.1306/D4268181-2B26-11D7-8648000102C1865D

Wang, Z., Yin, J., Hao, X., Wang, P., Zhang, Q., Lan, G., et al. (2021). Role of algae in travertine deposition revealed by microscale observations: a case study of Huanglong, Sichuan, China. *Carsologica Sin.* 40, 44–54. doi:10.11932/karst20210105

Witten, T. A., and Sander, L. M. (1981). Diffusion-limited aggregation, a kinetic critical phenomenon. *Phys. Rev. Lett.* 47, 1400–1403. doi:10.1103/physrevlett.47.1400

Wright, V. P., Beck, V. H., Sanz-Montero, M. E., Verrecchia, E. P., Freytet, P., Verrecchia, K. E., et al. (1996). Spherulites in calcrete laminar crusts; biogenic CaCO3 precipitation as a major contributor to crust formation; discussion and reply. *J. Sediment. Res.* 66, 1040–1044. doi:10.2110/jsr.66.1040

Wu, C., Yi, H., Hui, B., Xia, G., and Ma, X. (2014). A new sediment type of coated grain: oolitic sinter. *Sci. China Earth Sci.* 57, 2013–2024. doi:10.1007/s11430-014-4921-5

Zaichik, L. I., Alipchenkov, V. M., and Avetissian, A. R. (2009). Transport and deposition of colliding particles in turbulent channel flows. *Int. J. Heat Fluid Flow* 30, 443–451. doi:10.1016/j.ijheatfluidflow.2009.02.013

Zhang, J., Wang, H., Dong, L., and Zhao, D. (2012a). An analysis of travertine landscape degradation in Huanglong Ravine of Sichuan, a world's heritage site, and its causes and protection countermeasures. *Acta Geosci. Sin.* 33, 111–120. doi:10.3975/cagsb.2012.z1.14

Zhang, J., Wang, H., Liu, Z., An, D., and Dreybrodt, W. (2012b). Spatial-temporal variations of travertine deposition rates and their controlling factors in Huanglong Ravine, China - a world's heritage site. *Appl. Geochem.* 27, 211–222. doi:10.1016/j.apgeochem.2011.10.005

Zhang, K., Wang, H., and Ba, M. (2015). The research of geochemical characteristics and indicative significance for the source springs - a case of Huanglong Valley in Sichuan Province. *Adv. Mater. Res.* 3855, 423–427. doi:10.4028/www.scientific.net/amr.1094.423

Zhang, T., Dai, Q., An, D., Agustin, M. R., Li, Q. F., Astini, R. A., et al. (2023). Effective mechanisms in the formation of pool-rimstone dams in continental carbonate systems: the case study of Huanglong, China. *Sediment. Geol.* 455, 106486–12. doi:10.1016/j.sedgeo.2023.106486

Zinkernagel, U. (1978). Cathodoluminescence of quartz and its application to sandstone petrology. *Contributions Sediment. Geol.* 8, 54–58. doi:10.23689/fidgeo-1471